A Simple Method for Measuring the Size of Metal Nanoclusters in Solution

Anil V. Gaikwad, Peter Verschuren, Erika Eiser, and Gadi Rothenberg*

van 't Hoff Institute for Molecular Sciences, University of Amsterdam, Nieuwe Achtergracht 166, 1018 WV Amsterdam, The Netherlands

Received: June 12, 2006

The connection between quantum size effects and the surface plasmon resonance of metal nanoclusters is introduced and the pros and cons of in situ and ex situ cluster analysis methods are outlined. A new method for estimating the size of nanoclusters is presented. This method combines core/shell cluster synthesis, UV−visible spectroscopy, and Mie theory. The core/shell approach enables the estimation of metal cluster sizes directly from the UV−visible spectra, even for transition metal nanoclusters such as Pd that have no distinct surface-plasmon peak in UV−visible region. Pd/Au and Au/Pd core/shell clusters as well as Au−Pd alloy clusters are synthesized and used as test cases for simulations and spectroscopic measurements. The results of the simulations and UV−visible spectroscopy experiments are validated with transmission electron microscopy.

Introduction

The past decade has witnessed an explosion in the number of applications of metal nanoparticles. Catalysis,[1−6] optoelectronics,[7] fuel cells,[8−10] and drug delivery[11] are but a few examples. The reason for this rising interest in metallic and semiconductor nanoparticles (or "quantum dots") originates in their energy band structure that distinctly differs from the discrete energy levels of individual atoms and the continuous energy bands of bulk metals. Perhaps the most intriguing property is the characteristic metal plasmon frequency, ω_p. Clusters exhibit quantum-size confinement effects, observable as a shift in the bulk plasmon frequency. Hence, the UV−visible absorption spectrum contains information on the clusters' actual size. The worldwide interest in metal nanoparticles has resulted in a range of synthesis techniques, from "wet chemistry" and electrochemistry[12] to sonochemical synthesis and laser ablation.[13] These techniques can also be combined, enabling the synthesis of bimetallic particles with specific morphologies and compositions.[14−16] Bimetallic and core/shell type particles such as Pd/Pt,[17] Pt/Au,[18] Au/Pd,[19−24] Ag/Pd,[25] and Au/Ag[26−29] were also studied.

Understanding the clusters' size−, structure−, and composition−activity relationships is crucial. Cluster size is particularly important, because many of the special properties of nanoparticles are size-dependent. There are several methods for measuring cluster sizes, the most accurate of which are based on electron microscopy.[30] Transmission electron microscopy (TEM), for example, gives the size, shape, and particle size distribution. It is highly accurate and reliable, but also has some disadvantages: First, it is performed ex situ, so following the clusters during a reaction is difficult. Second, it requires expensive equipment and special sample preparation.

Alternatively, one can use other spectroscopic methods based on light absorption[31,32] or scattering.[33] We recently demonstrated the in situ monitoring of Pd cluster formation using UV−visible spectroscopy.[34] In some cases, however, there is a problem because the clusters do not show a well-defined peak in the UV−visible region. This is the case, for example, with palladium, a key metal in catalysis applications.[35,36]

To solve this problem, we present here a new and simple method for estimating palladium cluster sizes using UV−visible spectroscopy. In 1908, Mie studied the interaction of visible light with nanoparticles and proposed a method for estimating the particles' size.[37] Now, by coating the Pd clusters with a gold shell, and applying an extended version of Mie's theory, we overcome the problem that the plasmon maximum of Pd is outside the visible spectrum. We prepared Pd/Au and Au/Pd core/shell as well as Au−Pd alloy clusters in an organic solvent (to the best of our knowledge this is the first report for the synthesis of these types of nanoclusters in an organic solvent). In this work, we explain the concept behind our approach using these organosols as examples. Further we validate the UV−visible experiments and the theoretical models using TEM measurements. For clarity and completeness, we also give here a short theoretical basis as it applies to this problem.

Theory

When light hits a metal nanoparticle, the electric field polarizes the conduction electrons on the particle surface, generating a surface plasmon resonance (SPR).[38] The resonance spectra of dilute dispersions can be calculated with Mie theory.[37] Mie was the first to solve Maxwell's equation for light interacting with small spheres. Assuming that nanoparticles behave as frequency-dependent dielectric media, Mie's solution yields the particle extinction cross-section, C_{ext}.[39] For a dilute colloidal solution containing N particles per unit volume, the measured attenuation of the incoming light of intensity I_o over a path length d is given by,

$$A = \log\left(\frac{I_o}{I_d}\right) = NC_{ext}\left(\frac{d}{2.303}\right) \quad (1)$$

For spherical particles with a frequency-dependent dielectric function $\epsilon = \epsilon' + i\epsilon''$, embedded in a medium of dielectric function ϵ_m, C_{ext} is given by,

* Address correspondence to this author. E-mail: gadi@science.uva.nl. Fax: +31 20-525-5604.

10.1021/jp063644n CCC: $33.50
Published on Web 08/11/2006

$$C_{ext} = \frac{2\pi}{K^2}\sum(2n+1)\mathscr{R}(a_n + b_n) \quad (2)$$

where $K = 2\pi(\epsilon_m/\lambda)^{1/2}$ and $\mathscr{R}$ is the real part of the scattering coefficients a_n and b_n, which are functions of the cluster radius R and the wavelength λ in terms of Ricatti−Bessel functions. C_{ext} is often normalized per unit area as Q_{ext}:

$$Q_{ext} = \frac{C_{ext}}{\pi R^2} \quad (3)$$

If the nanoparticles are much smaller than the wavelength of light in the visible region (i.e., $2R \ll \lambda$) only the dipole oscillations contribute significantly to C_{ext},[40]

$$C_{ext} = \frac{24\pi^2 R^3 \epsilon_m^{3/2}}{\lambda}\frac{\epsilon''}{(\epsilon' + 2\epsilon_m)^2 + \epsilon''^2} \quad (4)$$

Such particles will respond as dielectric media in an optical field. Westcott et al. used bulk metal dielectric constants for determining the absorption and scattering cross-section of both solid and core/shell particles.[41] Most models assume that the dielectric constant depends on the particle size below an average $R \sim 10$ nm.

The most common models are based on size-dependent correction terms taken from bulk solid theories such as Drude's model.[42] According to this theory the real (ϵ') and imaginary (ϵ'') parts of the dielectric function are

$$\epsilon' = \epsilon_{inf} - \left[\frac{\omega_p^2}{(\omega^2 + \omega_d^2)}\right] \quad (5)$$

$$\epsilon'' = \frac{\omega_p^2 \omega_d}{[\omega(\omega^2 + \omega_d^2)]} \quad (6)$$

$$\omega_p^2 = \frac{pe^2}{m\epsilon_o} \quad (7)$$

Here ϵ_{inf} is the high-frequency dielectric constant due to interband and core transitions, ω_p is the bulk plasma frequency, p is the concentration of free electrons in the metal, m is the effective electron mass, and ϵ_o is the dielectric constant in a vacuum. ω_d is the relaxation or damping frequency. It is related to the mean-free path of the conduction electrons, l_{bulk}, the velocity of the electrons at the Fermi energy V_f, and the interaction parameter S by

$$\omega_d = \frac{Sv_f}{l_{bulk}} \quad (8)$$

$$\varpi_d = \omega_{dbulk} + \omega_d \quad (9)$$

When $R < l_{bulk}$, conduction electrons are also scattered by the surface. S is a theoretical parameter that depends on the medium surrounding the particle.[43] ω_{dbulk} signifies the bulk collision frequency. It embodies a number of physical processes such as electron−electron, electron−phonon, and electron−impurity interactions. In a semiclassical model, ω_d describes the elastic electron scattering from the surface of the nanoparticle and the interface damping due to adsorbate-induced resonant phases. Thus, summing the two terms in eq 9 is justified only for independent scattering processes.

Surface Plasmon Properties of Bimetallic Clusters. Wescott et al. showed that for core−shell bimetallic clusters, the SPR wavelength depends only on the ratio R_{total}:R_{core} and not on the absolute sizes.[41] Mie theory matches the electric and magnetic field boundary conditions at the core/shell and the shell/solvent interfaces. This determines the particles' scattering, absorption, and extinction cross-sections.[44] The deposition of metal atoms on metal particles (core/shell) causes dramatic optical shifts. Charge accumulation polarizes the particles, giving a blue shift. This blue shift distinguishes metal shell deposition from a simple stabilizing layer.[40]

In the following section, we apply the above theory to estimate C_{ext} for different core/shell bimetallic particles. One can then simulate the SPR spectra, and ultimately calculate the respective core and shell radii. This approach has some limitations:[45] It is not known a priori whether the bulk properties that are used as starting parameters are indeed valid for nanoparticles. There may be differences due to quantum mechanical confinement, surface melting, and surface adsorbates. Furthermore, the model's assumptions (e.g., sharp boundaries; no many-body effects) may be unreasonable. Therefore we also include an experimental validation of the SPR spectra.

Results and Discussion

Core/Shell Pd/Au Clusters. There are several methods for making core/shell clusters. Successive reduction in organic media was demonstrated by Kan and co-workers.[46] Huang and co-workers prepared Au/Pd clusters in reverse micelles.[47] We used a modification of the method described by Reetz and Maase,[14] preparing bimetallic clusters by successive reduction using tetraoctylammonium formate (TOAF) in an organic solvent. This method gives clusters with a narrow size distribution (±1 nm). We prepared three types of clusters: core/shell Au/Pd clusters, core/shell Pd/Au clusters, and Au−Pd alloy clusters. All experiments were performed in degassed solvents in an inert atmosphere. In a typical synthesis of core/shell Pd/Au clusters, the Pd^{2+} precursor was first dissolved in dimethylformamide (DMF) and subsequently reduced with 5 equiv of TOAF that also functioned as a stabilizer. Au^{3+} ions were then similarly reduced and deposited on the Pd cluster surface.

The clusters were then analyzed with UV−visible spectroscopy. Figure 1 shows the absorption spectra of Pd clusters and various core/shell Pd/Au combinations. Pure Pd clusters do not show a distinct peak in the visible region.[25] However, the suspension is dark brown. Adding Au^{3+} ions to the Pd cluster suspension changes the color to pink. Since the core radius of the Pd was the same, the increase in the amount of gold causes an increase in intensity with a marginal red shift. No SPR was observed for clusters with a Au:Pd molar ratio of less than 5:1, due to the effective d−d interband dampening of the Pd clusters.

In the above system, the Pd clusters are seed particles on which the Au shells grow. Note that Au^{3+} ions reduce more easily and thus get adsorbed preferably onto the Pd clusters instead of forming pure gold clusters. This process can be described as a surface-catalyzed growth of the Au shell.[48] Pd/Au core/shell particles are also energetically more stable.[49] These clusters show completely different spectral profiles both from the monometallic particles and from their mixtures (vide infra). The Pd core also dampens the Au surface plasmon absorption. As the Au^{3+} concentration increases, more Au^o atoms adsorb, increasing the Au shell thickness (Figure 1, top). The reason that the simulated spectra in Figure 1 are broader than the experimental spectra is that the dampening frequency ω_d is a

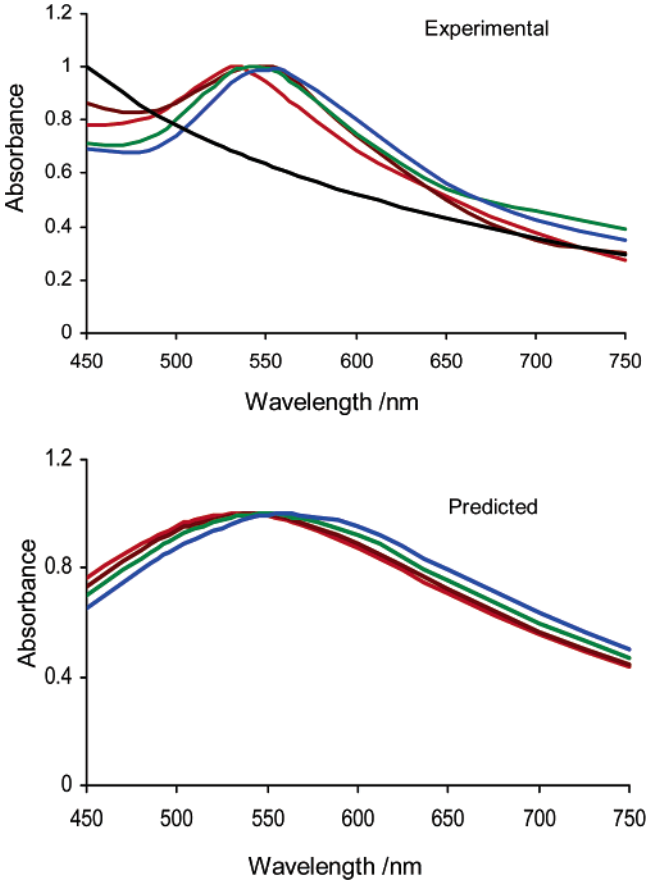

Figure 1. Zoom-in view of UV−visible spectra showing the experimental (top) and the calculated absorption spectra (bottom) for pure Pd clusters of 4 nm diameter (dark curve) and various core/shell Pd/Au clusters. The red, brown, green, and blue curves represent Au:Pd mole ratios of 5:1, 10:1, 15:1, and 20:1, respectively. All spectra are normalized at the plasmon absorption maximum.

TABLE 1: Numerical and Experimental Core Sizes and Shell Thicknesses of Various Pd/Au Core/Shell Clusters

entry	Au:Pd mole ratio	simulated Au shell thickness (nm)[a]	calcd Au shell thickness (nm)[b]	exptl λ_{max} (nm)	predicted λ_{max} (nm)
1	5:1	1.0	1.5	533	533
2	10:1	1.5	2.0	548	544
3	15:1	2.5	3.0	553	549
4	20:1	3.5	3.5	558	560

[a] Represents the simulated Pd core size of 4 nm and various Au shell thickness with Mie theory for coated particles. [b] Shows shell thickness calculated by using the density, molar weight, and initial molar ratio of Au and Pd.

given value taken from the literature.[50] However, the important point is that λ_{max} values match for the theory and the experiment.

Figure 1, bottom, shows the corresponding spectra that were calculated with use of our algorithms (see the methods section for details). A good correlation is observed when comparing these to the experimental spectra, and the results also fit well with TEM studies (vide infra). Table 1 shows the experimental and the simulated λ_{max} values. Shell thicknesses were calculated by using the density, molar weight, and initial molar ratio of Au and Pd. This is also in good agreement with the simulated shell thicknesses.

Determining the Cluster Size. We now apply Mie's theory to determine the size of the various Pd and Pd/Au clusters. First, an estimate of the Pd core diameter and the Au shell thickness

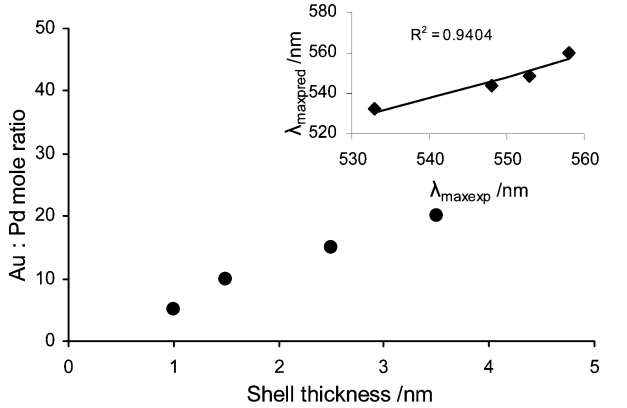

Figure 2. Simulated gold shell thicknesses obtained with varying Au:Pd mole ratios. The inset shows the fit between the experimental and the predicted surface plasmon maxima values.

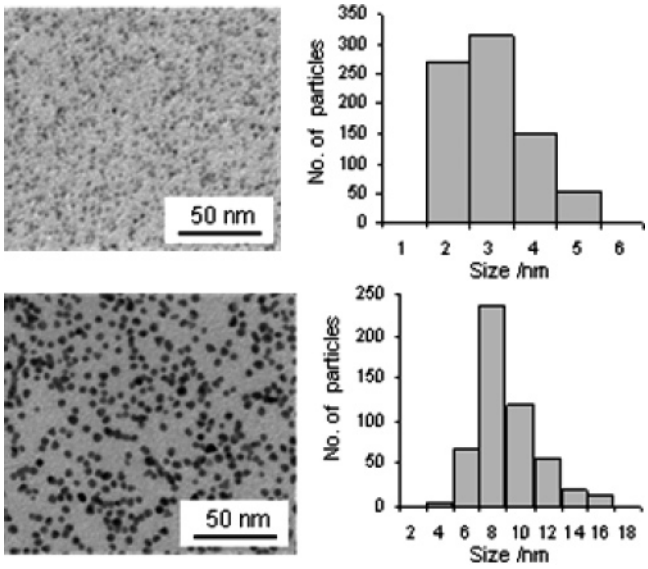

Figure 3. TEM micrographs of pure Pd clusters (top) and Pd/Au core/shell clusters (bottom) (the Au:Pd mole ratio is 20:1). The size distribution histograms are based on 800 particles counted.

was guessed as 4 and 3.5 nm, respectively (the Au:Pd mole ratio is 20:1), and the size-dependent dielectric constants for both metals were derived analytically. Then, the absorption spectra were predicted, and the simulated λ_{max} values for various shell thicknesses were compared to experimental values. The good correlation ($R^2 = 0.94$, see Figure 2) demonstrates the power of this approach.

TEM analysis confirmed that the cluster sizes were in the 3−4 nm range, matching the simulated Pd core sizes (Figure 3, top). Moreover the TEM micrographs of Pd/Au core/shell particles showed uniformly sized particles of 8 nm diameter. This increase in size can be clearly attributed to the Au shell on the Pd-cluster surface and the Au shell thickness matches well with simulated and calculated shell thicknesses (see entry 4 in Table 1).

Core/Shell Au/Pd Clusters. These clusters were prepared as above, reversing the order of the reduction steps. We synthesized Au cores of different diameters, examining the size effects. The core diameter depends strongly on the number of TOAF equivalents.[14] Figure 4 shows the absorption spectra of Au clusters prepared with different amounts of reducing and stabilizing agents. The surface plasmon resonance dependence on the particle size reflects several effects, including changes in the optical interband transition and changes of electronic band

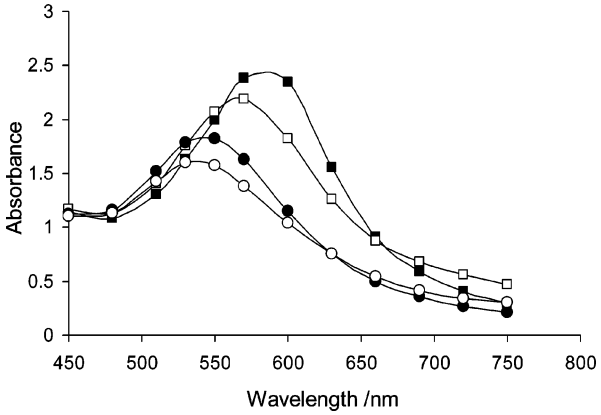

Figure 4. Experimental UV−visible absorption spectra (zoomed in) of pure Au clusters prepared with different mole equivalents of TOAF (■, □, ●, and ○ denote 8, 10, 12, and 14 mol equiv of TOAF, respectively). Spectra were taken every 1 nm. The symbols are shown for clarity.

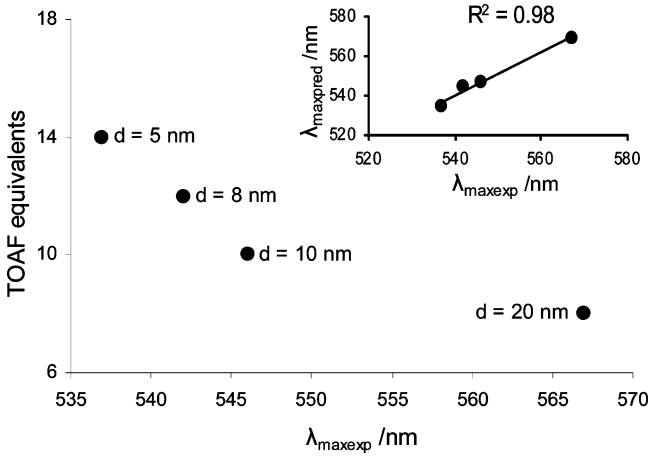

Figure 5. SPR λ_{max} wavelength for Au clusters of different sizes, prepared by reducing 0.5 mM $AuCl_3$ in DMF with different amounts of TOAF. The inset shows the correlation of the experimental and the predicted λ_{max} values.

structure and the ions adsorbed on the metal surface.[51,52] For gold clusters, the SPR shows a blue shift as the cluster size decreases.[53] Figure 5 shows the λ_{max} values of various Au clusters vs TOAF equivalents. With more TOAF, the solution changes from purple to red.

Following the UV−visible measurements we applied Mie's theory to determine the Au core sizes. For this, we first validated our algorithm using the theoretical correlation of λ_{max} and cluster size that was reported for Au clusters in water.[54] Then, we replaced the solvent parameters with those of DMF, obtaining the λ_{max} versus cluster size correlation in DMF. Finally, we used the same correlation to determine the Au cluster size based on the experimental λ_{max} values. This gave an excellent fit (R^2 = 0.98 for 4 observations, see Figure 5).

Pd^{2+} ions were then reduced and deposited on the Au surface. Figure 6 shows the UV−visible spectra for the core/shell Au/Pd clusters. When Pd coats Au-clusters it dampens the SPR, giving a broader peak. Smaller clusters showed less dampening and less spectral shift. Indeed, group 10 metals are known to dampen the SPR of group 11 metals in bimetallic clusters.[55] We also observed a blue shift in the Au absorption spectra in the presence of Pd.

Thicker Pd shells formed when larger Au cores were used. As the amount of gold was identical in all experiments, there must be fewer but larger clusters and consequently more Pd

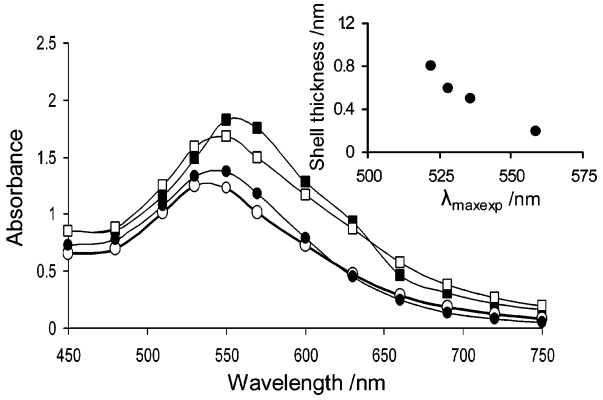

Figure 6. Zoom-in view showing the UV−visible spectra of core/shell Au/Pd clusters with different Au core sizes (■, □, ●, and ○ symbols denoting 20, 10, 8, and 5 nm, respectively) and Au:Pd mole ratio of 8:1. The inset shows the simulated SPR λ_{max} with respect to different Pd shell thicknesses. Spectra were taken every 1 nm. The symbols are shown for clarity.

TABLE 2: Numerical and Experimental Core Sizes and Shell Thicknesses of Various Pd/Au Core/Shell Clusters

entry	equiv of TOAF	predicted Au core size (nm)	simulated Pd shell thickness (nm)[a]	calcd Pd shell thickness (nm)[b]	exptl λ_{max} (nm)	predicted λ_{max} (nm)
1	8	20	0.8	1.1	558	559
2	10	10	0.6	0.5	537	536
3	12	8	0.5	0.4	532	528
4	14	5	0.2	0.3	532	522

[a] Simulated Pd-core size and Au-shell thickness with Mie theory for coated particles. [b] Shell thicknesses calculated by using the density, molar weight, and initial molar ratio of Au and Pd.

atoms per Au core. Our predicted spectra showed the same trend. For example, Pd shells, 0.8 and 0.6 nm thick, were predicted for Au cores 15 and 10 nm in diameter, respectively. Experimental and predicted λ_{max} values are given in Table 2. These predictions fit well with our experimental results (R^2 = 0.98 for 4 observations).

We then used transmission electron microscopy to validate our simulations. Figure 7 shows the TEM image of pure Au clusters (A and B). It shows an average cluster size around 14−16 nm. Parts C and D in Figure 7 show core/shell morphologies of Au/Pd clusters with a Pd layer thickness around 0.8−1 nm, which agrees well with our predicted results of 0.8 nm (see Table 2 entry 1). The Pd shell is brighter than the Au core due to the lower electron density in the d orbital. It is important to note that gold clusters were the same in both cases.

Au−Pd Bimetallic Clusters. These clusters were prepared by co-reducing $AuCl_3$ and $PdCl_2$ in different mole ratios of Au:Pd (4:1 to 26.6:1) with excess TOAF. Figure 8 shows the absorption spectra for respective alloy clusters. The increased amount of Pd shifts the λ_{max} more toward lower wavelength. Clusters with a Au:Pd mole ratio less than 4:1 do not show any significant plasmon absorption implying that the surface of Au−Pd bimetallic clusters has more Pd atoms.[56]

Since the reduction potential of Au is higher than that of Pd one can expect that the co-reduction of Au and Pd will result in the formation of Au/Pd core/shell type clusters instead of Au−Pd bimetallic clusters. Earlier studies of formation of Au/Pd core/shell and Au−Pd bimetallic clusters are not consistent, which could be attributed to the difference in the nucleation process. This was dependent on the kind of materials, the reaction media, and reducing and stabilizing agent.[57,58] Chen et

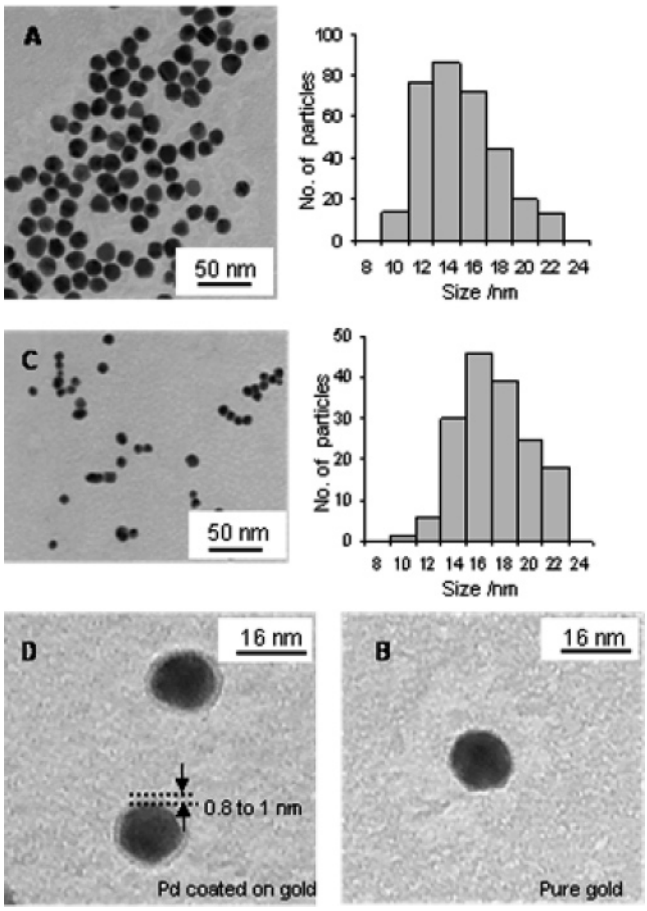

Figure 7. TEM micrograph of pure Au clusters (A and B) and Au/Pd core/shell clusters with a Au:Pd mole ratio of 8:1 (C and D), and the corresponding size distribution based on 300 particles counted.

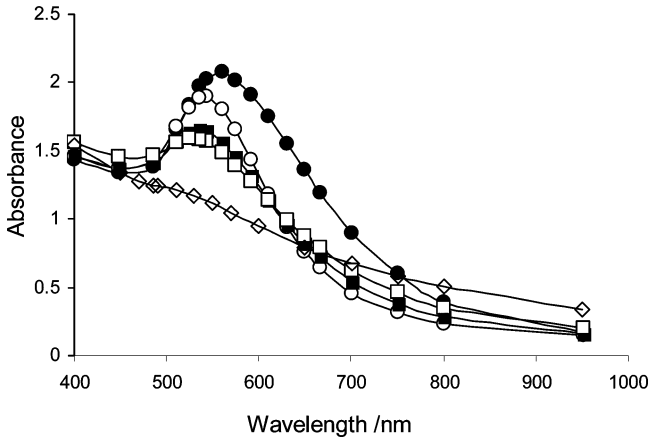

Figure 8. Zoom-in view of experimental UV−visible spectra of Au−Pd alloy clusters with various Au:Pd ratios (●, ○, ■, □, and ◇ symbols represent a Au:Pd mole ratio of 26.6:1, 16:1, 11.5:1, 8:1, and 4:1, respectively). Spectra were taken every 1 nm. The symbols are shown for clarity.

al. have shown that the formation of Au−Pd alloy clusters is possible.[47] Total Gibb's energy for the formation of nuclei might vary with compositions due to the different bond enthalpies or interactions of Au−Au, Pd−Pd, and Au−Pd. This can lead to a different number of atoms required for the formation of nuclei for different compositions. In our system we use TOAF, a very strong reducing agent. The reduction rates are so fast that the system becomes saturated with Pd° and Au° atoms. This increases the probability of collision between the atoms to form rapidly many nuclei and hence smaller clusters are formed.

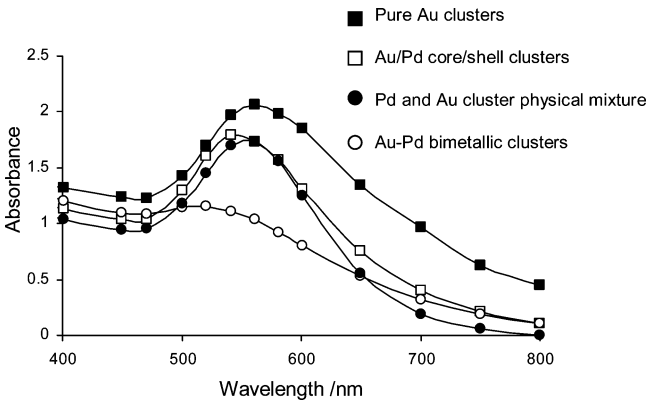

Figure 9. Zoom-in view of experimental UV−visible spectra of various types of clusters with a Au:Pd mole ratio of 8:1 (■, □, ●, and ○ symbols represent pure Au clusters, Au/Pd core shell structure, Pd and Au cluster mixture, and Au−Pd alloy clusters). Spectra were taken every 1 nm. The symbols are shown for clarity.

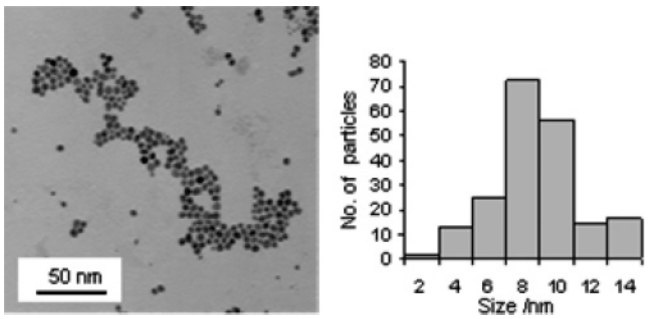

Figure 10. TEM micrographs of Au−Pd bimetallic clusters prepared with a Au:Pd mole ratio of 8:1. The size distribution histograms are based on 300 particles counted.

Another possibility is that, though the nuclei were composed of Au° atoms, the number of Au atoms needed to form a stable nucleus is reduced due to the presence of Pd atoms in the solution. Also Pd atoms will have a stronger influence on the total Gibb's energy of an atomic assembly when they are present in the nucleus rather than dispersed in the solution. Accordingly, the formation of Au−Pd bimetallic clusters composed of a mixture of Au° and Pd° atoms will be favored in our system. Subsequently, Au and Pd atoms co-deposited onto the nuclei and grew to their final size. Molecular dynamic studies of Pal and co-workers showed that Au−Pd bimetallic clusters are energetically more favorable.[49]

UV−visible spectra also show that these Au/Pd core/shell Au−Pd alloy clusters are different in nature. In Figure 9 we can observe that pure gold clusters show their surface plasmon maxima (λ_{max}) at 560 nm while the physical mixture of both clusters has the same λ_{max} but reduced absorption intensity. This proves that in the physical mixture the absorption characteristics of both individual clusters are maintained, excluding significant contributions from interparticle interaction. On the other hand, the Au/Pd core/shell type clusters show a λ_{max} shift to lower wavelengths at 540 nm, while Au−Pd alloy clusters show a remarkable blue shift with λ_{max} at 510 nm.

These observations can be further verified by the TEM micrographs. TEM images of Au/Pd core/shell and Au−Pd alloy clusters show clear differences in cluster size. Au−Pd alloy clusters are smaller and more uniform in size than the Au/Pd core/shell type clusters (see Figure 10). Both types of clusters were prepared with the same initial mole ratios of Au:Pd.

As both the d-band and the conduction electrons contribute to the SPR, most studies assume that the dielectric function of

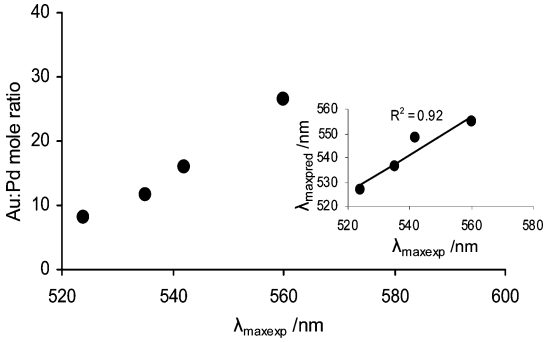

Figure 11. Experimental λ_{max} values for alloy clusters versus Au:Pd mole ratio. The inset shows the fit between the experimental and predicted λ_{max} values.

an alloy is a linear combination of the molar fractions. In this case ϵ is given by

$$\epsilon(x_{Au}) = (1 - x_{Au})\epsilon_{Pd} + x_{Au}\epsilon_{Au} \quad (10)$$

Then considering the above assumption we predicted the surface plasmon maxima λ_{max}. As shown in Figure 11 the predicted and experimental values match well.

Conclusions

By coating nonabsorbing palladium clusters with gold shells and employing a modified version of Mie's theory it is possible to estimate the Pd core size and the Au shell thickness directly from UV−visible spectra. The sample preparation is simple and the computational costs are low. The prediction results correlate well with experiment and are validated by TEM measurements. Although this technique is less accurate than electron microscopy, it presents a viable "rough and fast" alternative for estimating the size of homometallic and bimetallic nanoparticles.

Experimental Section

Materials and Instrumentation. UV−visible spectra were measured with a Hewlett-Packard 8453 spectrophotometer with a diode array detector and a quartz cuvette (Hellma Benelux, approximately 3.5 mL, path length 1 cm). Spectra were measured from 190 to 1100 nm at 1 nm resolution. Particle sizes were determined by transmission electron microscopy (TEM), using a JEOL model JEM-1200 EXII instrument operating at an accelerated voltage of 120 kV. Samples for TEM analysis were prepared by placing a drop of colloid on a 300 mesh carbon-coated copper grid and evaporating the solvent (50 °C, 750 mmHg). Unless stated otherwise, chemicals were purchased from commercial firms (>98% pure) and used as received. All solvents were degassed for 10 min with dry N_2 prior to use. Tetra-*n*-octylammonium formate (TOAF) was prepared according to a previously published procedure.[2] Stock solutions (10 mM) of Pd^{2+} and Au^{3+} ions were prepared by dissolving 17.7 mg of $PdCl_2$ or 33.0 mg of $AuCl_3$ in 10.00 mL of DMF (99.8%).

Procedures for Preparing Bimetallic and Alloy Clusters. *Au Clusters.* A Schlenk-type glass vessel equipped with a rubber septum and a magnetic stirrer was evacuated and refilled with N_2. The vessel was then charged with 2 mL of a 0.5 mM $AuCl_3$/DMF solution, and was stirred and heated at 65 °C for 1 h. Then, 80 μL of 100 mM TOAF in DMF was added in one portion into the vessel and the reaction was continued for 1 h. The reaction mixture was analyzed by UV−visible spectroscopy.

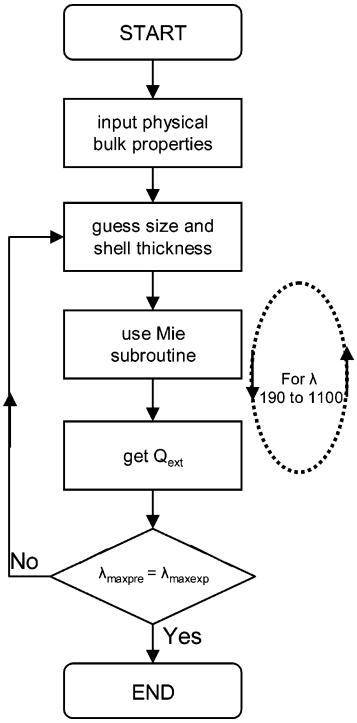

Figure 12. Flowchart of the algorithm for predicting the absorption spectra and the core and shell diameters of bimetallic nanoclusters.

Suspensions of gold clusters with different diameters were similarly prepared, using 100, 120, and 140 μL of 100 mM TOAF in DMF.

Pd Coated on Au Clusters. Au clusters with different diameters were first prepared according to a standard procedure. Then, 250 μL of 0.5 mM $PdCl_2$/DMF solution was injected and the vessel was heated for 1 h. These samples were analyzed by UV−visible spectroscopy.

Au Coated on Pd Clusters. A Schlenk-type glass vessel equipped with a rubber septum and a magnetic stirrer was evacuated and refilled with N_2. The vessel was then charged with 2 mL of 0.5 mM $PdCl_2$/DMF solution. This vessel was stirred and heated at 65 °C for 1 h. Then, 50 μL of 100 mM TOAF/DMF was added and the reaction was continued for 1 h. Subsequently, 500 μL of 10 mM $AuCl_3$/DMF was added (5:1 Au:Pd mole ratio) and reaction was continued for 1 h. This procedure was repeated with 1000, 1500, and 2000 μL of 10 mM $AuCl_3$/DMF, corresponding to 10:1, 15:1, and 20:1 Au:Pd mole ratios, respectively.

Au−Pd Alloy Clusters. A Schlenk-type glass vessel equipped with a rubber septum and a magnetic stirrer was evacuated and refilled with N_2. The vessel was then charged with 2 mL of 0.5 mM $AuCl_3$/DMF and 25 μL of 0.5 mM $PdCl_2$/DMF. After the solution was stirred at 65 °C for 10 min, 60 μL of 200 mM TOAF/DMF was added and the reaction was continued for 1 h. This procedure was repeated for 75, 125, 175, 250, and 450 μL of 0.5 mM $PdCl_2$/DMF for preparing Au−Pd alloy clusters with different Au:Pd mole ratios (26.6:1, 16:1, 11.5:1, 8:1, and 4:1 respectively).

Computational Methods. MATLAB[59] scripts were used for computing the metal clusters' size by applying Mie's theory (see the flowchart in Figure 12). The size-dependent dielectric function was determined from known physical bulk properties of both metals. These include the plasmon frequency ω_p, the bulk dampening frequency ω_d, the Fermi velocity v_f, the solvent refractive index n, the bulk dielectric constant ϵ_{bulk}, and mean free path l_{bulk}.[50,60,61] The absorption and scattering coefficients

a_n and b_n in the Ricatti−Bessel function were calculated with a modified version of Mätzler's subroutine.[62] Inserting these coefficients in eq 2 yields the Q_{ext} values for the wavelengths between 190 and 1100 nm. The algorithm works with guessed string values and optimizes the core diameter a and the shell diameter b, with the following assumptions: (i) all particles are spherical and have a uniform size distribution and (ii) the parameter $S \equiv 1$.

Acknowledgment. We thank Dr. T. Franssen-Verheijen (Wageningen University) for performing the TEM analysis and Marjo C. Mittelmeijer-Hazeleger for technical assistance. This research was funded by the Netherlands Organization for Scientific Research (NWO) Vernieuwingsimpuls program.

References and Notes

(1) Moreno-Mañas, M.; Pleixats, R. *Acc. Chem. Res.* **2003**, *36*, 638−643.
(2) Thathagar, M. B.; Beckers, J.; Rothenberg, G. *J. Am. Chem. Soc.* **2002**, *124*, 11858−11859.
(3) Zhong, C. J.; Maye, M. M. *Adv. Mater.* **2001**, *13*, 1507−1511.
(4) Toshima, N. *Pure Appl. Chem.* **2000**, *72*, 317−325.
(5) Conlon, D. A.; Pipik, B.; Ferdinand, S.; LeBlond, C. R.; Sowa, J. R., Jr.; Izzo, B.; Collins, P.; Ho, G.-J.; Williams, J. M.; Shi, Y.-J.; Sun, Y. *Adv. Synth. Catal.* **2003**, *345*, 931−935.
(6) LeBlond, C. R.; Andrews, A. T.; Sun, Y.; Sowa, J. R., Jr. *Org. Lett.* **2001**, *3*, 1555−1557.
(7) Rothenberg, E.; Kazes, M.; Shaviv, E.; Banin, U. *Nano Lett.* **2005**, *5*, 1581−1586.
(8) Chuang, S. S. C. *Catalysis* **2005**, *18*, 186−198.
(9) Bönnemann, H.; Richards, R. M. *Eur. J. Inorg. Chem.* **2001**, 2455−2480.
(10) Paulus, U. A.; Endruschat, U.; Feldmeyer, G. J.; Schmidt, T. J.; Bönnemann, H.; Behm, R. J. *J. Catal.* **2000**, *195*, 383−393.
(11) Polato, L.; Benedetti, L. M.; Callegaro, L. *J. Drug Targeting* **1994**, *2*, 53−59.
(12) Reetz, M. T.; Winter, M.; Breinbauer, R.; Thurn-Albrecht, T.; Vogel, W. *Chem. Eur. J.* **2001**, *7*, 1084−1094.
(13) For reviews see: (a) El-Shall, M. S.; Li, S. *Adv. Met. Semiconduct. Clusters* **1998**, *4*, 115−177. (b) Okada, T.; Maeda, M. *Recent Res. Dev. Appl. Phys.* **2004**, *7*, 535−551.
(14) Reetz, M. T.; Maase, M. *Adv. Mater.* **1999**, *11*, 773−777.
(15) Son, S. U.; Jang, Y.; Park, J.; Na, H. B.; Park, H. M.; Yun, H. J.; Lee, J.; Hyeon, T. *J. Am. Chem. Soc.* **2004**, *126*, 5026−5027.
(16) Durán Pachón, L.; Thathagar, M. B.; Hartl, F.; Rothenberg, G. *Phys. Chem. Chem. Phys.* **2005**, *8*, 151−157.
(17) Wang, Y.; Toshima, N. *J. Phys. Chem. B* **1997**, *101*, 5301−5306.
(18) Chandler, B. D.; Pignolet, L. H. *Catal. Today* **2001**, *65*, 39−50.
(19) Mizukoshi, Y.; Fujimoto, T.; Nagata, Y.; Oshima, R.; Maeda, Y. *J. Phys. Chem. B* **2000**, *104*, 6028−6032.
(20) Remita, H.; Etcheberry, A.; Belloni, J. *J. Phys. Chem. B* **2003**, *107*, 31−36.
(21) Hu, J.-W.; Zhang, Y.; Li, J.-F.; Liu, Z.; Ren, B.; Sun, S.-G.; Tian, Z.-Q.; Lian, T. *Chem. Phys. Lett.* **2005**, *408*, 354−359.
(22) Wu, M.-L.; Chen, D.-H.; Huang, T.-C. *Langmuir* **2001**, *17*, 3877−3883.
(23) Nath, S.; Praharaj, S.; Panigrahi, S.; Ghosh, S. K.; Kundu, S.; Basu, S.; Pal, T. *Langmuir* **2005**, *21*, 10405−10408.
(24) Harpeness, R.; Gedanken, A. *Langmuir* **2004**, *20*, 3431−3434.
(25) Michaelis, M.; Henglein, A.; Mulvaney, P. *J. Phys. Chem.* **1994**, *98*, 6212−6215.
(26) Moskovits, M.; Srnova-Sloufova, I.; Vlckova, B. *J. Chem. Phys.* **2002**, *116*, 10435−10446.
(27) Chen, D.-H.; Chen, C.-J. *J. Mater. Chem.* **2002**, *12*, 1557−1562.
(28) Ehler, T. T.; Noe, L. J. *Langmuir* **1995**, *11*, 4177−4179.
(29) Kariuki, N. N.; Luo, J.; Maye, M. M.; Hassan, S. A.; Menard, T.; Naslund, H. R.; Lin, Y.; Wang, C.; Engelhard, M. H.; Zhong, C.-J. *Langmuir* **2004**, *20*, 11240−11246.
(30) For reviews see: (a) Jose-Yacaman, M.; Avalos-Borja, M. *Catal. Rev. Sci. Eng.* **1992**, *34*, 55−127. (b) Baker, R. T.; Bernal, S.; Calvino, J. J.; Perez-Omil, J. A.; Lopez-Cartes, C. *Nanotechnol. Catal.* **2004**, *2*, 403−426.
(31) Link, S.; El-Sayed, M. A. *J. Phys. Chem. B* **1999**, *103*, 4212−4217.
(32) Belotelov, V. I.; Carotenuto, G.; Nicolais, L.; Pepe, G. P.; Zvezdin, A. K. *Eur. Phys. J. B* **2005**, *45*, 317−324.
(33) Eah, S.-K.; Jaeger, H. M.; Scherer, N. F.; Wiederrecht, G. P.; Lin, X.-M. *Appl. Phys. Lett.* **2005**, *86*, 031902.
(34) (a) Wang, J.; Boelens, H. F. M.; Thathagar, M. B.; Rothenberg, G. *ChemPhysChem* **2004**, *5*, 93−98. (b) Gaikwad, A. V.; Rothenberg, G. *Phys. Chem. Chem. Phys.* **2006**, *8*, 3669−3675.
(35) Phan, N. T. S.; Gill, C. S.; Nguyen, J. V.; Zhang, Z. J.; Jones, C. W. *Angew. Chem., Int. Ed.* **2006**, *45*, 2209−2212.
(36) Lang, H. G.; Maldonado, S.; Stevenson, K. J.; Chandler, B. D. *J. Am. Chem. Soc.* **2004**, *126*, 12949−12956.
(37) Mie, G. *Ann. Phys* **1908**, *25*, 377.
(38) Creighton, J. A.; Eadon, D. G. *J. Chem. Soc., Faraday Trans.* **1991**, *87*, 3881−3891.
(39) Bohren, C. F.; Huffman, D. R. *Absorption and scattering of light by small particles*; John Wiley & Sons: New York, 1983.
(40) Mulvaney, P. *Langmuir* **1996**, *12*, 788−800.
(41) Westcott, S. L.; Jackson, J. B.; Radloff, C.; Halas, N. J. *Phys. Rev. B* **2002**, *66*, 155431.
(42) Zhu, J. *Phys. Lett. A* **2005**, *339*, 466−471.
(43) Pinchuk, A.; Kreibig, U.; Hilger, A. *Surf. Sci.* **2004**, *557*, 269−280.
(44) Oldenburg, S. J.; Hale, G. D.; Jackson, J. B.; Halas, N. J. *Appl. Phys. Lett.* **1999**, *75*, 1063−1065.
(45) Shahbazyan, T. V.; Perakis, I. E.; Bigot, J. Y. *Phys. Rev. Lett.* **1998**, *81*, 3120−3123.
(46) Kan, C. X.; Cai, W. P.; Li, C. C.; Zhang, L. D.; Hofmeister, H. *J. Phys. D: Appl. Phys.* **2003**, *36*, 1609−1614.
(47) Wu, M. L.; Chen, D. H.; Huang, T. C. *Langmuir* **2001**, *17*, 3877−3883.
(48) Mandal, M.; Kundu, S.; Ghosh, S. K.; Pal, T. *J. Photochem. Photobiol., A* **2004**, *167*, 17−22.
(49) Liu, H. B.; Pal, U.; Medina, A.; Maldonado, C.; Ascencio, J. A. *Phys. Rev. B* **2005**, *71*, 075403.
(50) Ferraton, J. P.; Leveque, G.; Robin-Kandare, S. *J. Phys. F: Met. Phys.* **1975**, *5*, 1433−1438.
(51) Link, S.; El-Sayed, M. A. *Int. Rev. Phys. Chem.* **2000**, *19*, 409−453.
(52) Kreibig, U.; Genzel, L. *Surf. Sci.* **1985**, *156*, 678−700.
(53) Wilcoxon, J. P.; Williamson, R. L.; Baughman, R. *J. Chem. Phys.* **1993**, *98*, 9933−9950.
(54) Soennichsen, C.; Franzl, T.; Wilk, T.; von Plessen, G.; Feldmann, J. *New J. Phys.* **2002**, *4*, 93.1−93.8.
(55) Sánchez-Ramírez, J. F.; Pal, U. *Superficies y Vacío* **2001**, *13*, 114−116.
(56) Toshima, N.; Harada, M.; Yamazaki, Y.; Asakura, K. *J. Phys. Chem.* **1992**, *96*, 9927−9933.
(57) Yonezawa, T.; Toshima, N. *J. Chem. Soc., Faraday Trans.* **1995**, *91*, 4111−4119.
(58) Esumi, K.; Shiratori, M.; Ishizuka, H.; Tano, T.; Torigoe, K.; Meguro, K. *Langmuir* **1991**, *7*, 457−459.
(59) *Matlab* version 6.1; Mathworks, Natick USA.
(60) Johnson, P. B.; Christy, R. W. *Phys. Rev. B* **1972**, *6*, 4370.
(61) Chang, S. S.; Shih, C. W.; Chen, C. D.; Lai, W. C.; Wang, C. R. C. *Langmuir* **1999**, *15*, 701−709.
(62) Mätzler, C. MATLAB Functions for Mie Scattering and Absorption; Institut für Angewandte Physik, 2002.